© 2015. Published by The Company of Biologists Ltd | Development (2015) 142, 4151-4157 doi:10.1242/dev.128058

RESEARCH ARTICLE

Flow dynamics control the location of sprouting and direct elongation during developmental angiogenesis

Siavash Ghaffari[1,2], Richard L. Leask[2] and Elizabeth A. V. Jones[1,2,3,*]

ABSTRACT

Angiogenesis is tightly controlled by a number of signalling pathways. Although our understanding of the molecular mechanisms involved in angiogenesis has rapidly increased, the role that biomechanical signals play in this process is understudied. We recently developed a technique to simultaneously analyse flow dynamics and vascular remodelling by time-lapse microscopy in the capillary plexus of avian embryos and used this to study the hemodynamic environment present during angiogenic sprouting. We found that sprouts always form from a vessel at lower pressure towards a vessel at higher pressure, and that sprouts form at the location of a shear stress minimum, but avoid locations where two blood streams merge even if this point is at a lower level of shear stress than the sprouting location. Using these parameters, we were able to successfully predict sprout location in quail embryos. We also found that the pressure difference between two vessels is permissive to elongation, and that sprouts will either change direction or regress if the pressure difference becomes negative. Furthermore, the sprout elongation rate is proportional to the pressure difference between the two vessels. Our results show that flow dynamics are predictive of the location of sprout formation in perfused vascular networks and that pressure differences across the interstitium can guide sprout elongation.

KEY WORDS: Angiogenesis, Hemodynamics, Time-lapse microscopy, Micro-particle image velocimetry, Computational fluid dynamics

INTRODUCTION

The vasculature is the first organ to form during development and it adapts to the onset of blood flow in part by forming new blood vessels through angiogenesis. The ability to control angiogenesis has important therapeutic applications for many diseases. Anti-angiogenic treatments used to treat tumours lead to transient vessel normalisation, which causes a reduction in tumour invasiveness and better delivery of chemotherapeutic drugs (Carmeliet and Jain, 2011). In wet macular degeneration, defective angiogenesis leads to the formation of leaky vessels that damage the eye and lead to vision loss. Anti-angiogenic therapies can effectively stop and sometimes reverse the progression of macular degeneration (Tah et al., 2015). As such, there is significant interest in understanding the signals that induce or inhibit angiogenesis.

In the adult vasculature, endothelial cells exist in a quiescent state wherein little proliferation occurs (Hanahan and Folkman, 1996; Hobson and Denekamp, 1984). Normal physiological levels of shear stress maintain endothelial cells in a quiescent state by inducing cell cycle arrest (Lin et al., 2000) and strengthening tight junctions (Lin et al., 2000). For sprouting to occur, however, endothelial cells must re-enter the cell cycle (Bai et al., 2014), loosen their attachment to neighbouring cells (Lampugnani and Dejana, 2007), degrade the local basement membrane (Siefert and Sarkar, 2012) and then invade the tissue. Although shear stress is known to affect many of these pathways, very little is known about the effects of shear stress on angiogenesis. Two groups recently developed micro-machined flow cells that enabled them to alter shear stress and interstitial flow as endothelial cells sprout (Galie et al., 2014; Song and Munn, 2011). Both groups found that interstitial flow enhanced angiogenesis, however, one found that shear stress inhibited sprouting (Song and Munn, 2011), whereas the other found that it induced sprouting (Galie et al., 2014). Using an embryonic model, our group has demonstrated that increasing blood viscosity, which increases shear stress, results in a decrease in vascular density (Chouinard-Pelletier et al., 2013). We showed by time-lapse microscopy that this occurs because of a decrease in sprouting angiogenesis. Changing viscosity, however, also altered other hemodynamic parameters such as the pressure drop through the network. These studies establish a role for flow dynamics in angiogenesis but a better understanding of the hemodynamic environment present *in vivo* during sprouting is needed to identify the causal stimuli.

The vascular network must not only deliver oxygen and nutrients to tissues, but it must also be hemodynamically efficient. If a new vessel forms in a hemodynamically inefficient location, then a high resistance to flow will be present and limited flow will pass through that vessel. The production of a hemodynamically efficient vascular network can occur either by excessive production of blood vessels followed by the pruning of inefficient vessels, or by sprouting of new vessels in hemodynamically efficient locations in the first place. Though vascular networks do overproduce vessels and prune inefficient ones (Pries and Secomb, 2014), this does not negate the possibility of a bias at the site of sprout initiation in perfused vascular networks. It therefore makes physiological sense that the forces created by blood flow could influence the angiogenic process.

RESULTS

Sprout location can be predicted based on flow dynamics

To study the role that flow dynamics play in the process of angiogenesis, we used a technique to simultaneously image vessel morphology and flow dynamics by time-lapse microscopy in the capillary plexus of avian embryos undergoing vascular remodelling (Ghaffari, et al., 2015). We injected Alexa Fluor 488-labelled acetylated low-density lipoprotein (AF488-AcLDL), which specifically labels endothelial cells and macrophages (Brown et al., 1980; Hallmann et al., 1987). AF488-AcLDL labels not

[1]Lady Davis Institute for Medical Research, McGill University, 3755 Chemin de la Côte-Ste-Catherine, Montréal, Quebec H3T 1E2, Canada. [2]Department of Chemical Engineering, McGill University, 3610 University Street, Montréal, Quebec H3A 0C5, Canada. [3]Department of Cardiovascular Science, KU Leuven, UZ Herestraat 49, Box 911, Leuven 3000, Belgium.

*Author for correspondence (liz.jones@med.kuleuven.be)

Received 2 July 2015; Accepted 29 October 2015

Development (2015) 142, 4151-4157 doi:10.1242/dev.128058

only perfused vessels, but also sprouting endothelial cells. We then injected red fluorescent microspheres to follow blood flow dynamics and imaged the microspheres with a high-speed camera. We analysed the pattern of blood flow present during sprouting in the arterial plexus of three quail embryos as well as the venous plexus of three additional quail embryos, for a total of 6 time-lapse recordings (Fig. 1A). Early in vascular development, a spatial separation exists such that the rostral capillary plexus is venous and the caudal plexus is arterial. The motion of the microspheres was analysed using a technique called micro-particle image velocimetry (μPIV) to calculate the velocity of the blood. Micro-PIV was only used to make velocity measurements in straight vessel segments that led in and out of a region of interest. These measurements were then used as the input for a computational fluid dynamic solver to calculate flow in the entire region of interest, around the growing sprout. Flow dynamics were analysed starting 30 min before the sprout was visible and continued until the new vessel lumenised and carried flow (Fig. 1B, yellow arrowheads). The computational solver calculates blood velocity in the entire region of interest from the μPIV inputs (Fig. 1C,D), as well as calculating shear stress, pressure drop and vorticity (Movies 1-3).

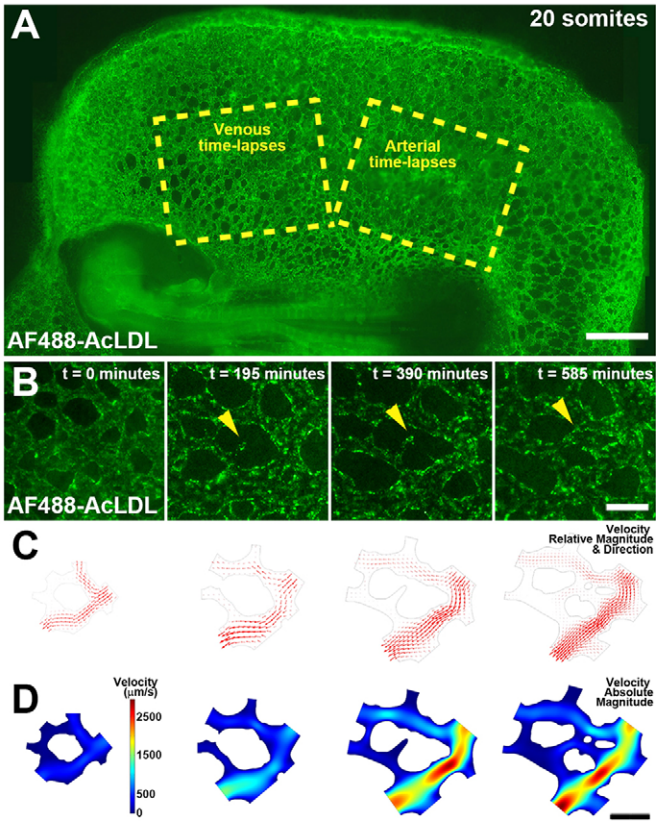

Fig. 1. Fluid dynamic analysis over a 10 h time-lapse period. All time-lapse movies started with embryos at 12-14 somites (or Hamburger Hamilton Stage 11) and embryonic endothelial cells labelled with AF488-AcLDL were imaged for a total of 12-16 h. (A) The flow dynamics during sprouting angiogenesis were analysed for a total of six embryos, three in the arterial region of the capillary plexus and three in the venous region. (B) Analysis of the time-lapse recordings was performed on data from 30 min before the sprout was first observed until the new vessel lumenised and flow was present in the new vessel. Yellow arrowheads indicate sprout. Blood flow velocity and pattern was determined for the entire cardiac cycle, however, only values for peak systole are presented (C,D; Movie 1). By combining viscosity estimates with the velocity profiles in the vessels, the relative pressure (Movie 2), shear stress (Movie 3) and vorticity (Movie 3) were calculated. Scale bars: 1000 μm in A; 100 μm in B-D.

We first investigated the relationship between flow parameters and the location of sprout initiation. We found that sprouts consistently formed from vessels at lower pressure towards vessels at higher pressure (Fig. 2, n=6/6 embryos, P=0.014). The contour plots of relative pressure 30 min before sprout formation are presented, both for the arterial (Fig. 2A) and the venous (Fig. 2C) regions of the plexus. The location and direction of sprouting are identified by the black arrows (Fig. 2A,C) as observed in the green images of vascular morphology after the sprout has formed (Fig. 2B,D, yellow arrowheads). The average pressure difference between the initiation site and the opposite vessel (i.e. the one towards which the sprout is extended) was of the same order of magnitude in all embryos. Pressure differences were normalised by the distance between the two vessels. The average value was +2.1 Pa/mm (s.e.m.=0.09, n=3) for arteries and +1.7 Pa/mm (s.e.m.=0.09, n=3) for veins. Though sprouts formed from lower towards higher pressure vessels, the location and direction of sprouting was not at the site of the maximum pressure difference in any of the time-lapse experiments.

Shear stress has been shown to play a significant role in controlling angiogenesis. We therefore investigated the level of shear stress on the endothelium when sprouting initiated (i.e. 30 min prior to sprout appearance, Fig. 3). Shear stress contour plots just prior to sprouting for the three arterial embryos are shown in Fig. 3A, whereas Fig. 3B shows the level of shear stress with respect to distance along the endothelium. The black lines and arrows in Fig. 3A indicate the arc length represented in the x-axis of Fig. 3B (x=0 at the bottom of the arrow). Shear stress levels were plotted for a subsection of the lower pressure region; however plots of the entire region are available in Fig. S1. We found that for all arterial time-lapse recordings, the location of sprouting could be identified by a local minimum in shear stress (Fig. 3B, sprouting location indicated by black arrows, n=3/3 embryos). Our previous results had indicated that shear stress inhibited sprouting angiogenesis in the venous but not the arterial plexus (Chouinard-Pelletier et al., 2013). In our venous time-lapse experiments, the sprout location was not associated with any specific pattern or level of shear stress (data not shown). One occurred at a minimum; the second at a midpoint; and the third was very close to the point with highest level of shear stress in the region. Therefore, in veins, our current results do not support a correlation between the level of shear stress and the sprouting location.

Though sprouts in the arterial plexus formed at a local minimum in shear stress, this was not always the absolute minimum. We investigated flow patterns at all shear stress minima (Fig. 4A, blue arrow represents sprouting location, orange arrow represents the second shear stress minimum in Embryo 1). We observed that non-sprouting shear stress minima occurred in regions where two streams of blood flow merged (Fig. 4A, n=3/3 embryos). Vorticity is the angular velocity of a fluid, and convergence or divergence of streams results in a sign change in the vorticity. Regions where streams converge can clearly be identified in the contour plots of the vorticity because the vorticity changes from a positive to a negative value (Fig. 4B, orange arrow indicating region with a change from red to blue). Though there is significant vorticity in this region, this occurs because of the angular velocity of the fluid that results from the streams converging and not because of the presence of recirculation. We plotted shear stress (Fig. 4C,E,G) and vorticity (Fig. 4D,F,H) for the entire region at lower pressure. If points where the vorticity passes through zero are excluded from the analysis, then the lowest minimum in shear stress defines the location of sprouting (n=3/3 embryos, P=0.010).

Development (2015) 142, 4151-4157 doi:10.1242/dev.128058

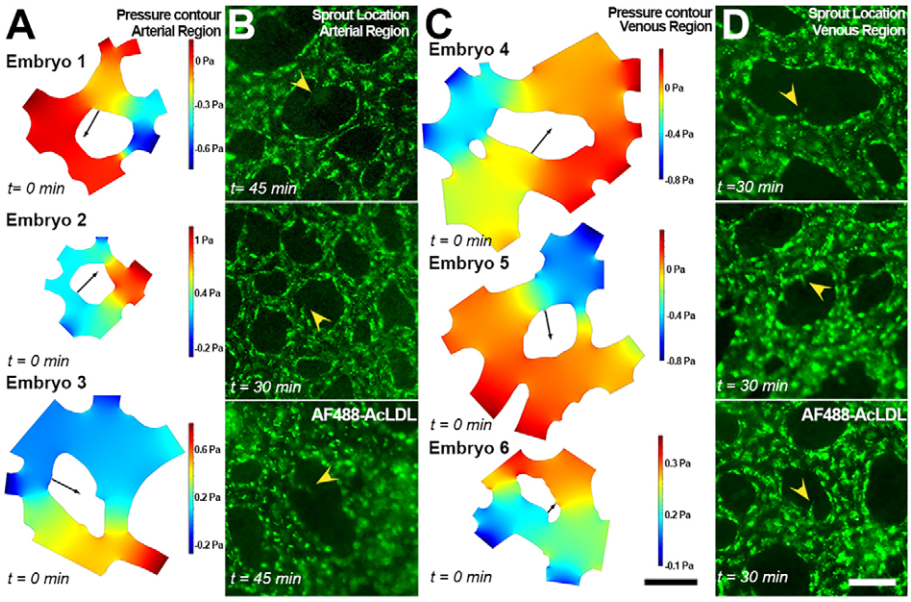

Fig. 2. Sprouts form from vessels at lower pressure towards vessels at higher pressure. (A,C) Contour plots for the relative pressure in all six embryos followed by time-lapse microscopy are presented (3 arterial, A,B; 3 venous, C,D). Plots represent calculated relative pressure just prior to the onset of sprouting (30 min before the sprout is visible). Sprout location is shown by yellow arrowheads in the AF488-AcLDL-labelled green image of the vascular network (B,D) and indicated on contour plots by black arrows (A,C). A positive pressure differential between the two vessels was always present, both for arteries (A) and veins (C). Scale bars: 100 µm.

We next tested whether we could use these observations to predict sprouting location. We analysed flow dynamics prior to sprouting in the arterial region of four new embryos (Fig. 5). The region and time point that were analysed were chosen by one author but analysed by a different author, making the analysis blind to sprouting location. Predicted sprouting location was restricted to the bottom 50% of pressure values (Fig. 5A). Within the lower pressure region, we identified all shear stress minima and all locations where vorticity equalled zero (Fig. 5B). Excluding locations with zero vorticity, the lowest minimum was chosen as the predicted sprout location (Fig. 5B). The actual sprout location was then assessed (Fig. 5C), blind to the predicted sprout location, based on the green images of vascular morphology and the location of x=0 from the pressure contour plots. In all embryos (n=4/4 embryos, P=0.001), we were able to correctly predict sprout location. Without VEGF, however, sprouts would not form at all. It is important to note that, in our system, fluid dynamics did not predict which avascular regions would sprout, but instead the flow predicted where along the vessel wall sprouting would occur. We did find that the sprouting avascular regions were larger on average than non-sprouting avascular regions (Fig. S2A, n=10 for each, P=0.012). Given the observed spread within the data (Fig. S2B), the size of the avascular region alone cannot predict which regions will sprout.

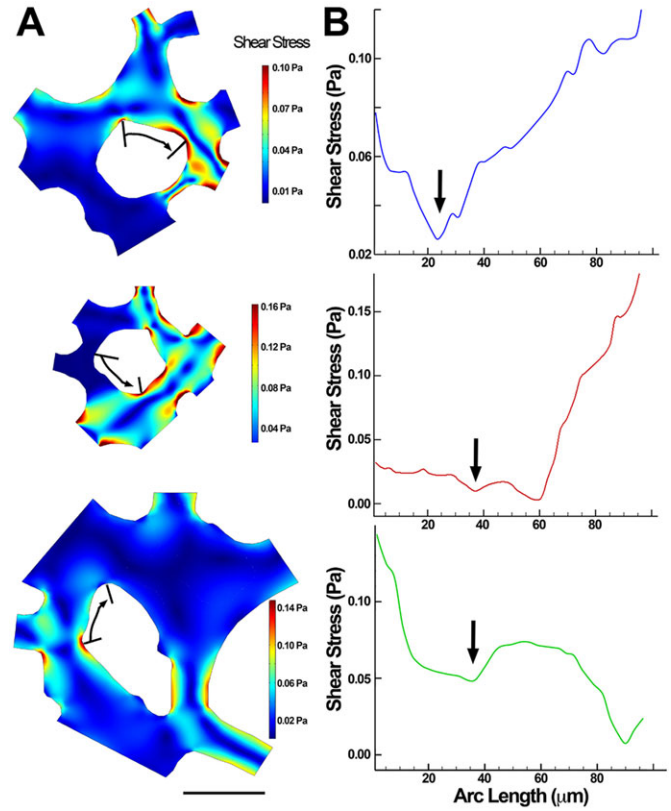

Fig. 3. Sprouts form in a local minimum of shear stress. (A) Contour plots show shear stress levels for a subsection of the lower pressure region in the arterial vascular network of three embryos, 30 min prior to the sprout being visible. Black lines and arrows indicate the starting location and the direction for the arc length that is plotted as the x-axis in B. Data for the entire arc length is presented in Fig. S1. (B) Sprout location is indicated by a black arrow in the plot of shear stress versus arc length (24 µm for Embryo 1, 36 µm for Embryo 2, 36 µm for Embryo 3). Sprouting location represents a local minimum in shear stress for all three embryos. Scale bar: 100 µm.

Sprout elongation rate is proportional to the pressure difference between the two vessels

We frequently observed that sprouts would extend and retract before finally connecting to form a lumenised vessel (Fig. 6A, yellow arrows indicate direction of sprout movement), as has been observed in other model systems (Murakami et al., 2006). We plotted the elongation rate of the sprouts (Fig. 6B), measured by the displacement of the tip of the sprout between two frames, and compared this to changes in the three analysed hemodynamic parameters in our system. We observed that regression of the sprout occurred when the difference in pressure between the vessels became negative (Fig. 6C, n=3/3 embryos). We therefore plotted the elongation rate with respect to the pressure difference between the two vessels (Fig. 6D). Negative elongation rates represent sprout regression. We found a logarithmic relationship between the elongation rate and the pressure difference between the vessels (Fig. 6E). The non-linear regression gave an r^2 value of 0.82 (Fig. 6D), whereas the linear regression on the semi-ln plot gave an r^2 value of 0.87 (Fig. 6E, P<0.05). Thus, these results show that

Development (2015) 142, 4151-4157 doi:10.1242/dev.128058

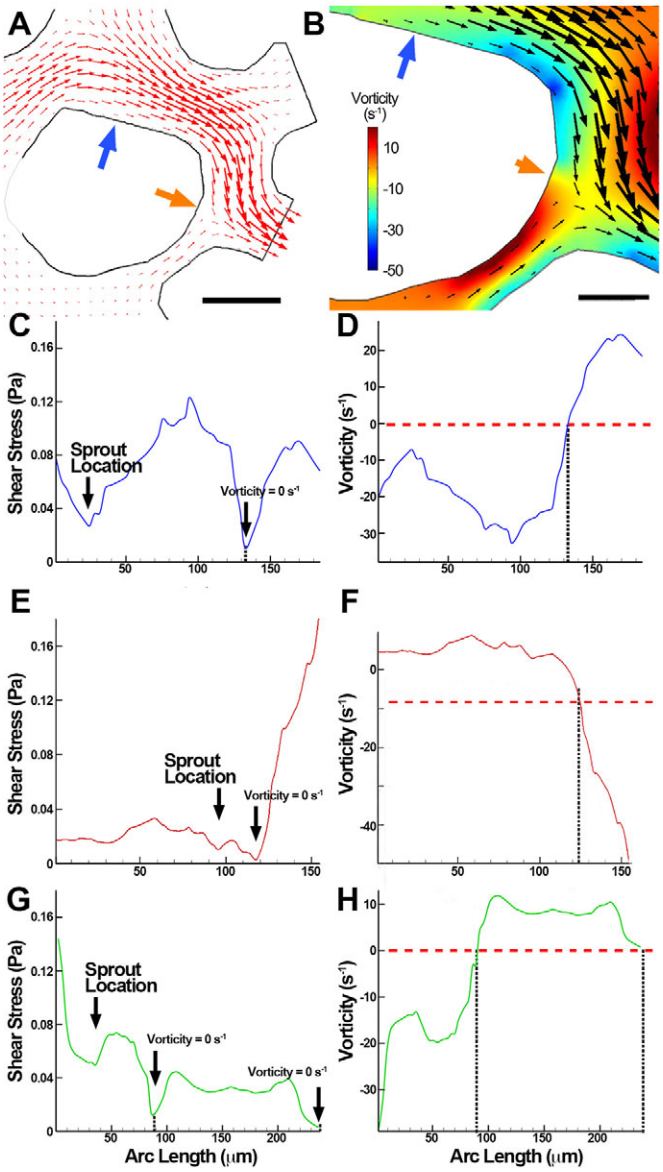

Fig. 4. Sprouting does not occur at locations where two blood flow streams merge. (A,B) Velocity plots show locations of low shear stress points (blue and orange arrows) with respect to the flow patterns present. The blue arrow indicates sprouting location and the orange arrow indicates a non-sprouting shear stress minimum. The non-sprouting minimum occurs at a point where streams merge and a change in sign of the vorticity is present (B, blue to red transition in contour plot). (C-H) Shear stress and vorticity plots for Embryo 1 (C,D), Embryo 2 (E,F) and Embryo 3 (G,H). In Embryo 1, two shear stress minima are present at 22 µm and 132 µm (C, plots show half the total arc length representing the lower 50% of pressure values). The sprout forms at the first shear stress minimum (22 µm, or blue arrow in A,B). The latter shear stress minimum (132 µm, orange arrow in A,B) represents a point where streams merge and a change in sign in vorticity is present (D). The exclusion of sprouting from locations where vorticity is zero was consistently observed in all three embryos. Dotted black lines indicate locations where vorticity is equal to zero. Scale bar: 100 µm.

there is a significant association between the rate of elongation and the pressure difference between two vessels.

In some time-lapse experiments, we observed the direction of elongation changing dynamically in relation to pressure differences between two vessels. This occurred in two of the three arterial time-lapse recordings. In one example, taken from Embryo 2 of the arterial time-lapse recordings (Fig. 7), the sprout was extending at time point 210 min (Fig. 7A, yellow arrowhead). The middle panels show the contour maps for relative pressure in this region with the extending sprout labelled in black (Fig. 7B). At 210 min, the pressure difference between the vessels in the sprouting direction was positive (Fig. 7C). The flow pattern changed, resulting in a negative pressure difference in the direction of sprouting by 240 min. The sprout retracted slightly and then changed direction towards a point that resulted in a positive pressure difference (t=270 min, Fig. 7C). Sprouts did not necessarily extend along the maximum pressure difference. They would continue in the same direction as long as the pressure difference was positive but changed direction or regressed when the pressure difference was negative. As such, the pressure difference was permissive rather than instructive.

DISCUSSION

We show that flow dynamics have a significant effect on the sprouting location, the direction of sprouting and the rate of elongation in arterial vascular networks. We found that sprouts only form from a vessel at low pressure towards a vessel at higher pressure, such that there is a positive pressure difference at the sprouting location. Within the lower pressure region, sprouts formed at the lowest minimum in shear stress once locations where streams merge were excluded.

Our results do not, however, show that fluid dynamics control when a sprout will form, but rather where they are likely to form. Previous *in vitro* work on sprouting and shear stress had shown that shear stress could inhibit VEGF-induced sprouting (Song and Munn, 2011). Similarly, our results suggest that the formation of a sprout within an avascular region is initiated by non-hemodynamic parameters, but that the fluid dynamic parameters define the position of that sprout.

Our results support that shear stress is inhibitory to sprouting, as we and others have found (Chouinard-Pelletier et al., 2013; Song and Munn, 2011; Tressel et al., 2007). More recently, another group published that shear stress induced rather than inhibited sprouting (Galie et al., 2014). It is possible that both extremes are permissive to sprouting. Both low (<10 dyn/cm^2) and pathologically high shear stress (>50 dyn/cm^2) result in increased cell turnover by stimulating both apoptosis (Davies et al., 1986; Dolan et al., 2011) and proliferation (Davies et al., 1986; Metaxa et al., 2008; Sho et al., 2003). Physiological levels of shear stress, by contrast, induce endothelial cell quiescence. Our analysis indicates that the physiologically relevant signal during development is the presence of lower shear stress levels. Under pathologically high shear stress, we cannot exclude that shear stress could be pro-angiogenic.

Our previous results had indicated that shear stress only inhibited sprouting in veins but not in arteries (Chouinard-Pelletier et al., 2013). Similarly, others had found that steady shear stress inhibited sprouting in venous or capillary endothelial cell types (i.e. HUVECs and HMECs) but not in arterial endothelial cell types (BAECs) (Tressel et al., 2007). Our current results, however, indicate the opposite. Our previous results were based on an embryonic model in which we altered shear stress levels by altering the viscosity of the blood (Chouinard-Pelletier et al., 2013). Increased viscosity not only changes shear stress but would also create a more drastic pressure drop within the vascular network, such that pressure differences between vessels in the veins might be smaller. An alternative explanation is that increasing the shear stress levels throughout the embryo resulted in an arterialisation of the venous network. Though we cannot differentiate between these

Development (2015) 142, 4151-4157 doi:10.1242/dev.128058

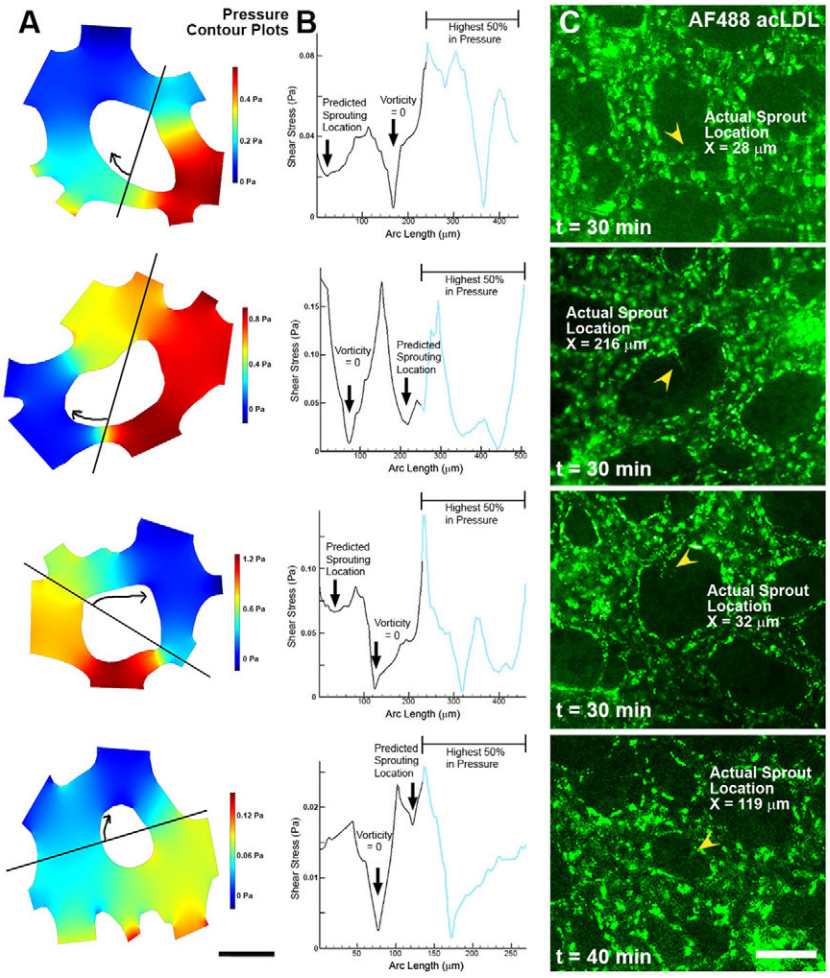

Fig. 5. Application of the three hemodynamic parameters can predict sprouting location in perfused networks. The hemodynamic parameters for sprouting in four embryos were analysed blind to sprout location. (A) Only the lowest 50% of relative pressure in each embryo were considered as possible sprouting locations. The base of each arrow in A indicates the start of the *x*-axis in B. (B) Shear stress plots of Embryos 1-4. Locations where the vorticity is equal to zero were identified and excluded from the analysis of shear stress minima. The lowest remaining shear stress minimum was chosen as the predicted sprouting location. (C) When compared with the actual sprouting location identified in the AF488-AcLDL-labelled green image of the vascular network, in all four cases the sprouting location was successfully identified (*n*=4/4 embryos). Scale bar: 100 μm.

possibilities, it remains clear that the arterial and venous identity of the bed affects the relationship between shear stress and sprouting dynamics.

Our results also indicated that though locations where two flows merge create points of low shear stress and large pressure differences, sprouts do not initiate from these points. We investigated flow during the cardiac cycle to identify whether flow reversals or oscillations were present at these locations, but found that the flow remained unidirectional throughout the cardiac cycle. Whether vorticity affects endothelial cells has never been studied, but it seems improbable as vorticity is not a force but rather a measure of the rate of rotation of the fluid elements. The endothelium is a continuous layer connected by gap junctions and endothelial cells can sense gradients in shear stress (Dolan et al., 2011; Rouleau et al., 2010). Points at which there is a change in sign in the vorticity are surrounded by shear stress vectors on either side that are in opposite directions. As such, these points do not have a zero gradient in shear stress (i.e. where the magnitude and sign of shear stress is the same on both sides of the sprouting location) and do not represent true minima in shear stress.

We find that the pressure difference between vessels, and not the absolute value of the relative pressure, is proportional to elongation rate. It is improbable that the hydrostatic pressure itself is biologically active in our model. The pressure differences that we observed in these vessels are several orders of magnitude smaller than the levels of hydrostatic pressure that have been shown to be biologically active (Sato and Ohashi, 2005). The pressure difference between the vessels does, however, control the rate at which fluids exit a vessel and therefore regulates the interstitial flow patterns. Interstitial flow alone, without a VEGF gradient, can promote sprouting in an *in vitro* system (Song and Munn, 2011). Interstitial flow will modify the distribution of growth factors and metabolites in the interstitial tissue, and it was previously shown that a gradient of VEGF in the presence of interstitial flow was more effective at promoting sprouting than either alone (Song and Munn, 2011). As such, rather than sprout elongation being controlled by pressure directly, current *in vitro* evidence would indicate that the interstitial flow is the instructive parameter. We are currently developing computational models to study the distribution of angiogenic cues and the range of interstitial flow to further investigate this phenomenon.

MATERIALS AND METHODS

Simultaneous imaging of vascular remodelling and blood flow dynamics

All experimental methods were performed in accordance with the relevant guidelines on animal use. A detailed description of the methods was previously presented (Ghaffari, et al., 2015). Fertilised quail eggs (*Cortunix japonica*) were incubated at 37°C and ∼60% humidity until they reached a developmental stage of 12-14 somites or Hamburger Hamilton 11 (HH11). The embryos were injected intravascularly with labelling dyes using a picospritzer III micro-injector (General Valve Corporation). Alexa Fluor 488 acetylated low-density lipoprotein (AF488-AcLDL, Invitrogen, L-23380) was used to label endothelial cells and PEGylated polystyrene microspheres (0.5 μm diameter red, Invitrogen, Amino-PEG, Laysan Bio)

Development (2015) 142, 4151-4157 doi:10.1242/dev.128058

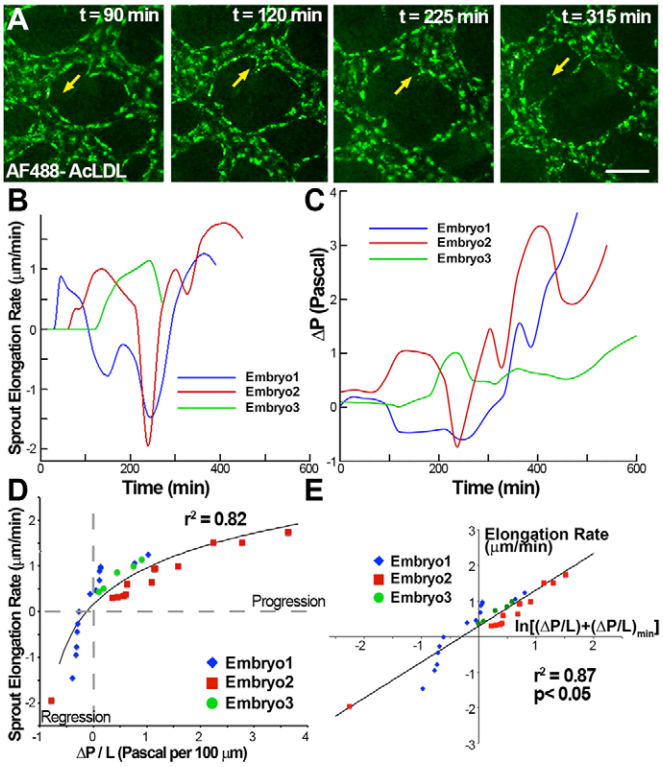

Fig. 6. The rate of elongation is proportional to the magnitude of the pressure differential. (A) Sprouts were often observed to extend and regress (yellow arrows indicate direction of sprout motion). (B,C) When sprout elongation rate (B) and pressure differential (C) were plotted with respect to time, periods of sprout regression were found to occur when negative pressure differentials were present in all three arterial plexuses. (D) In a direct correlation plot, the rate of elongation was found to strongly correlate with pressure differential between the vessels. (E) Plotting the data on a semi-ln plot demonstrated a logarithmic relationship between these quantities. Pressure differentials were normalised by L, the distance between the two vessels. Scale bar: 100 μm.

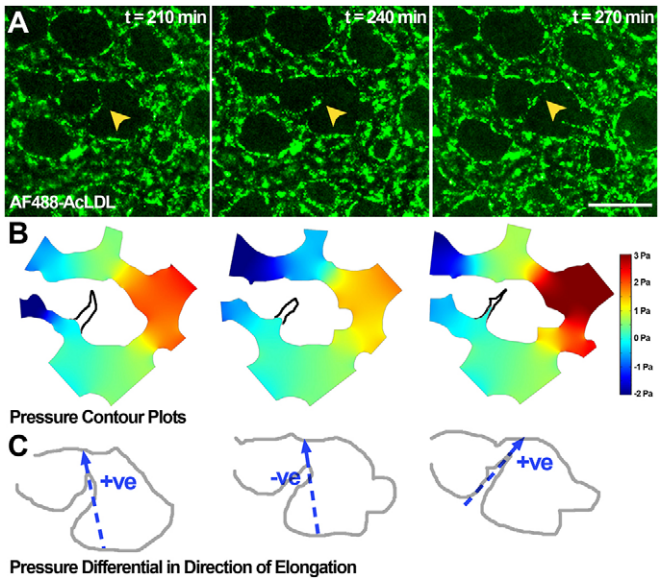

Fig. 7. Sprouts will change direction to follow a positive pressure differential. (A) A sprout (yellow arrowhead) can be observed extending and then changing direction over a period of 1 h in images of the AF488-AcLDL-labelled vascular network. (B,C) Contour plots (B) indicate changing pressure within the vessels during this time period (unlumenised sprout drawn in black). The sprout is initially extending in a direction of positive pressure differential (C). As the pressure differential becomes negative, the sprout regresses slightly (240 min) before beginning to extend in a new direction where the pressure differential is positive. Changes in sprouting direction were observed in two of three embryos analysed. Scale bar: 100 μm in A-C.

were injected to image the flow dynamics. Embryo culture for time-lapse microscopy was done as previously described (Al-Roubaie et al., 2012). Embryos were imaged on an upright fluorescence microscope equipped with an Axiocam MRC for images of the vascular morphology (AF488-AcLDL) and a high-speed camera (Photron FASTCAM Ultima APX-RS) for images of the microsphere motion. Endothelial cells were imaged with a 5× objective lens every 15 min. Blood flow dynamics were imaged with a 10× objective lens at 250 fps for two full cardiac cycles (equivalent to 2 s of imaging time), once every 2 h.

Image processing and μPIV analysis

The green image of the vasculature and the 500 red images of the microsphere motion were flattened into a single image to identify the walls of perfused vessels. A median filter was applied to the flattened image and then the image was thresholded to obtain a binary image used as the 'image mask' (for additional details, see Ghaffari et al., 2015). The image mask was applied to each individual frame of the microsphere motion. The centreline of each vessel was found by skeletonising the image mask. A Canny algorithm for edge detection was applied to the image mask to identify vessel walls. The local vessel diameter was obtained based on the vessel centreline and the vessel walls. Flow inlets and outlets were chosen far from branch points. Micro-PIV was used to calculate velocity waveforms based on the microsphere motion during the cardiac cycle at these inlets and outlets. Because the Reynolds number for the flow is very close to one and the Womersley number is less than one (Jones et al., 2004), entrance length effects are on the order of microns and a fully developed velocity profile was assumed for the μPIV analysis.

Computational fluid dynamics

The vascular geometry obtained by image processing and the inlet/outlet velocities acquired by μPIV were imported into a computational fluid dynamic (CFD) solver. The governing equations inside the vessels (i.e. continuity and momentum equations for laminar, non-Newtonian, incompressible flow) were solved using a finite elements method (FEM) in COMSOL Multiphysics 4.4. The unsteady form of the momentum equations was used for flow inside the vessels to take into account the effects of blood flow pulsatility. The viscosity of blood was adjusted for embryonic stage, vessel diameter and shear rate as previously described (Ghaffari, et al., 2015). From N inlets and outlets, the flow rates at $N-1$ points were set as boundary conditions. For the last outlet, the fully developed boundary condition was applied at the extended outlet of the domain (dependent on Reynolds number), i.e. $(\partial/\partial_x)=0$. Mesh generation and solution was performed by COMSOL. The domain was meshed with extremely fine free triangular meshes. Two convergence criteria were used: first, a mass flux residual of less than 10^{-8} for each control volume; second, $(|\phi_{i+1}-\phi_i|)/|\phi_{i+1}|\leq 10^{-10}$ for all time steps where ϕ represents v_x or v_y (flow velocities in x and y directions) and i is the number of iterations.

Statistical analysis

For formation of sprouts on the lower pressure side, a chi-squared test was used to compare the probability of sprouts always forming on one side (n=6) with the probability of sprouts forming randomly (n=3 and n=3, for low and high pressure side, respectively). For sprout location at shear stress minima, the arc length was divided into six possible sprouting locations and a chi-squared test was used to evaluate the probably that sprouts would form in one location rather than randomly in all six locations. The value of six was chosen as a conservative value as it would equate to ∼30 μm of arc length. Sprouts form within microns of predicted shear stress minima. For the relationship between pressure difference and elongation rate, we tested for co-integration using a Dickey–Fuller test and established that the relationship between the variables was stationary (P<0.05).

Development (2015) 142, 4151-4157 doi:10.1242/dev.128058

Competing interests

The authors declare no competing or financial interests.

Author contributions

S.G. performed experiments, developed methodology, analysed data and wrote the paper. R.L.L. developed methodology, analysed data and edited the paper. E.A.V.J. performed experiments, developed methodology, analysed data and wrote the paper.

Funding

E.A.V.J. was supported by grants from the Sick Kids Foundation of Canada [NI12-029] and a grant from Life Science Research Partners. R.L.L. was supported by a grant from the Canadian Institute of Health Research [MOP-119292]. S.G. was supported by a McGill Engineering Doctoral Award.

Supplementary information

Supplementary information available online at
http://dev.biologists.org/lookup/suppl/doi:10.1242/dev.128058/-/DC1

References

Al-Roubaie, S., Hughes, J. H., Filla, M. B., Lansford, R., Lehoux, S. and Jones, E. A. V. (2012). Time-lapse microscopy of macrophages during embryonic vascular development. *Dev. Dyn.* **241**, 1423-1431.

Bai, Y., Leng, Y., Yin, G., Pu, X., Huang, Z., Liao, X., Chen, X. and Yao, Y. (2014). Effects of combinations of BMP-2 with FGF-2 and/or VEGF on HUVECs angiogenesis in vitro and CAM angiogenesis in vivo. *Cell Tissue Res.* **356**, 109-121.

Brown, M. S., Basu, S. K., Falck, J. R., Ho, Y. K. and Goldstein, J. L. (1980). The scavenger cell pathway for lipoprotein degradation: specificity of the binding site that mediates the uptake of negatively-charged LDL by macrophages. *J. Supramol. Struct.* **13**, 67-81.

Carmeliet, P. and Jain, R. K. (2011). Molecular mechanisms and clinical applications of angiogenesis. *Nature* **473**, 298-307.

Chouinard-Pelletier, G., Jahnsen, E. D. and Jones, E. A. V. (2013). Increased shear stress inhibits angiogenesis in veins and not arteries during vascular development. *Angiogenesis* **16**, 71-83.

Davies, P. F., Remuzzi, A., Gordon, E. J., Dewey, C. F., Jr and Gimbrone, M. A., Jr. (1986). Turbulent fluid shear stress induces vascular endothelial cell turnover in vitro. *Proc. Natl. Acad. Sci. USA* **83**, 2114-2117.

Dolan, J. M., Meng, H., Singh, S., Paluch, R. and Kolega, J. (2011). High fluid shear stress and spatial shear stress gradients affect endothelial proliferation, survival, and alignment. *Ann. Biomed. Eng.* **39**, 1620-1631.

Galie, P. A., Nguyen, D.-H. T., Choi, C. K., Cohen, D. M., Janmey, P. A. and Chen, C. S. (2014). Fluid shear stress threshold regulates angiogenic sprouting. *Proc. Natl. Acad. Sci. USA* **111**, 7968-7973.

Ghaffari, S., Leask, R. L. and Jones, E. A. V. (2015). Simultaneous imaging of blood flow dynamics and vascular remodelling during development. *Development* **142**, 4158-4167.

Hallmann, R., Feinberg, R. N., Latker, C. H., Sasse, J. and Risau, W. (1987). Regression of blood vessels precedes cartilage differentiation during chick limb development. *Differentiation* **34**, 98-105.

Hanahan, D. and Folkman, J. (1996). Patterns and emerging mechanisms of the angiogenic switch during tumorigenesis. *Cell* **86**, 353-364.

Hobson, B. and Denekamp, J. (1984). Endothelial proliferation in tumours and normal tissues: continuous labelling studies. *Br. J. Cancer* **49**, 405-413.

Jones, E. A. V., Baron, M. H., Fraser, S. E. and Dickinson, M. E. (2004). Measuring hemodynamic changes during mammalian development. *Am. J. Physiol. Heart Circ. Physiol.* **287**, H1561-H1569.

Lampugnani, M. G. and Dejana, E. (2007). Adherens junctions in endothelial cells regulate vessel maintenance and angiogenesis. *Thromb. Res.* **120** Suppl. 2, S1-S6.

Lin, K., Hsu, P.-P., Chen, B. P., Yuan, S., Usami, S., Shyy, J. Y.-J., Li, Y.-S. and Chien, S. (2000). Molecular mechanism of endothelial growth arrest by laminar shear stress. *Proc. Natl. Acad. Sci. USA* **97**, 9385-9389.

Metaxa, E., Meng, H., Kaluvala, S. R., Szymanski, M. P., Paluch, R. A. and Kolega, J. (2008). Nitric oxide-dependent stimulation of endothelial cell proliferation by sustained high flow. *Am. J. Physiol. Heart Circ. Physiol.* **295**, H736-H742.

Murakami, T., Suzuma, K., Takagi, H., Kita, M., Ohashi, H., Watanabe, D., Ojima, T., Kurimoto, M., Kimura, T., Sakamoto, A. et al. (2006). Time-lapse imaging of vitreoretinal angiogenesis originating from both quiescent and mature vessels in a novel ex vivo system. *Invest. Ophth. Vis. Sci.* **47**, 5529-5536.

Pries, A. R. and Secomb, T. W. (2014). Making microvascular networks work: angiogenesis, remodeling, and pruning. *Physiology* **29**, 446-455.

Rouleau, L., Rossi, J. and Leask, R. L. (2010). The response of human aortic endothelial cells in a stenotic hemodynamic environment: effect of duration, magnitude, and spatial gradients in wall shear stress. *J. Biomech. Eng.* **132**, 071015.

Sato, M. and Ohashi, T. (2005). Biorheological views of endothelial cell responses to mechanical stimuli. *Biorheology* **42**, 421-441.

Sho, E., Komatsu, M., Sho, M., Nanjo, H., Singh, T. M., Xu, C., Masuda, H. and Zarins, C. K. (2003). High flow drives vascular endothelial cell proliferation during flow-induced arterial remodeling associated with the expression of vascular endothelial growth factor. *Exp. Mol. Pathol.* **75**, 1-11.

Siefert, S. A. and Sarkar, R. (2012). Matrix metalloproteinases in vascular physiology and disease. *Vascular* **20**, 210-216.

Song, J. W. and Munn, L. L. (2011). Fluid forces control endothelial sprouting. *Proc. Natl. Acad. Sci. USA* **108**, 15342-15347.

Tah, V., Orlans, H. O., Hyer, J., Casswell, E., Din, N., Sri Shanmuganathan, V., Ramskold, L. and Pasu, S. (2015). Anti-VEGF therapy and the retina: an update. *J. Ophthalmol.* **2015**, 627674.

Tressel, S. L., Huang, R.-P., Tomsen, N. and Jo, H. (2007). Laminar shear inhibits tubule formation and migration of endothelial cells by an angiopoietin-2-dependent mechanism. *Arterioscler. Thromb. Vasc. Biol.* **27**, 2150-2156.

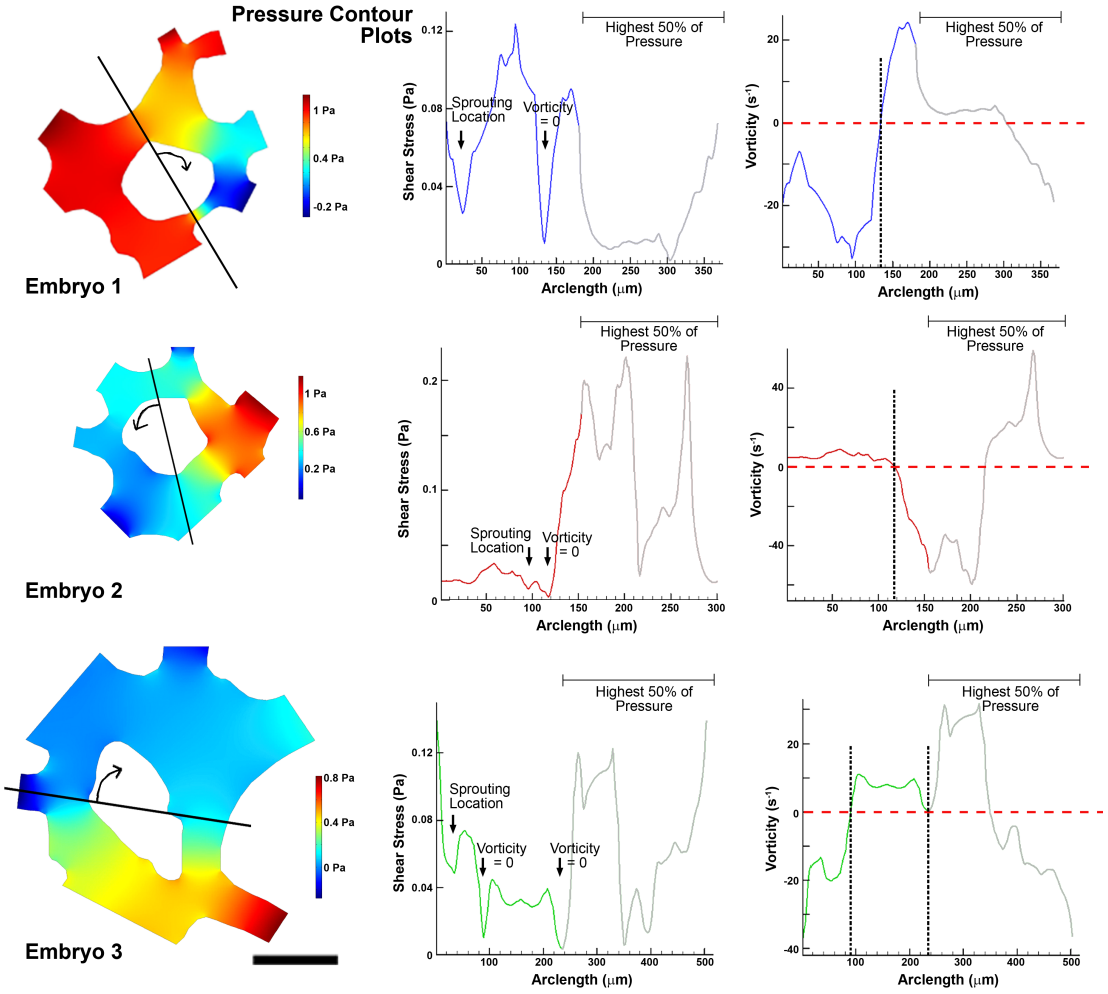

Fig. S1. Hemodynamic data for entire arclength at the time point 30 minutes before sprout is visible. Pressure contours for each embryo are presented. Shear stress and vorticity values for the entire contour are shown, with the region at higher pressure indicated by a grey line rather than a coloured line.

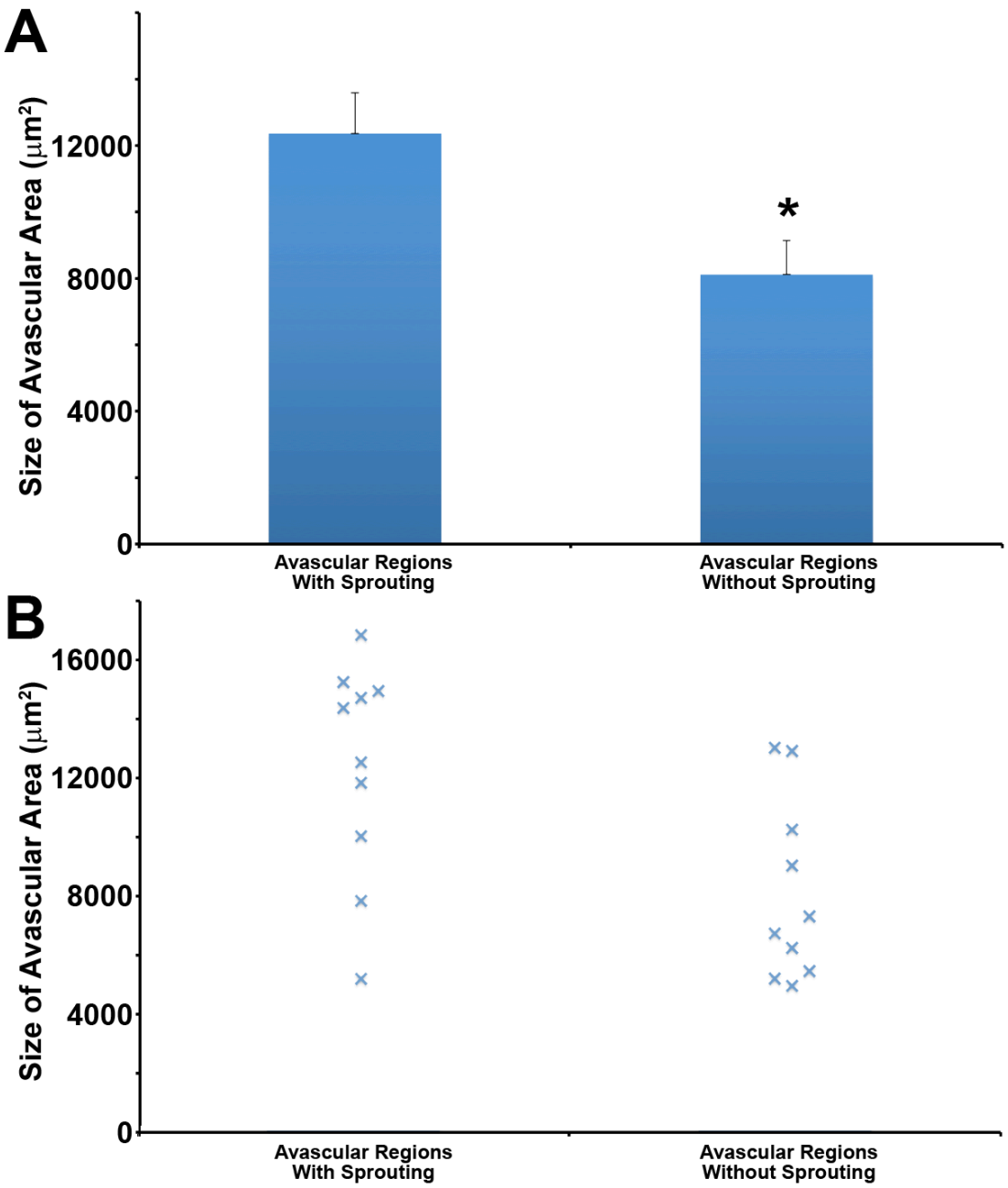

Fig. S2. Area of avascular region is larger in sprouting than non-sprouting location. The area of avascular regions at the time of sprouting was calculated, and compared to the area of avascular regions, at the same time point, that never sprouted during the entire time-lapse recording (A). Though sprouting avascular regions were larger than non-sprouting region ($p<0.05$), size of the region alone cannot predict which avascular regions sprout due to the large spread of the data.

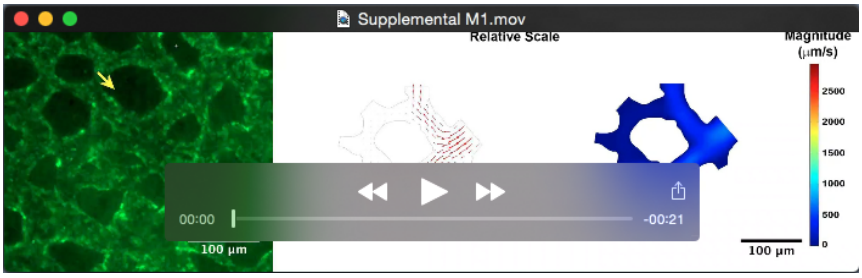

Movie 1. Blood velocity analysis around sprouting angiogenesis. Results of the analysis of blood velocity changes during sprouting are presented. The left panel shows the endothelial cell behaviour during the time period of analysis. The centre panel shows the velocity vectors for the blood flow during peak systole in the network. Velocity vectors are sized based on the maximum velocity at that specific time point (i.e. scale is relative). The right panel shows the absolute velocity magnitude during peak systole in these vessels during angiogenic sprouting. All scale bars represent 100 μm.

Movie 2. Pressure changes during sprouting angiogenesis. Results of the pressure calculations during sprouting are presented. The left panel shows the endothelial cell behaviour during the time period of analysis. The centre panel shows the relative pressure, where red represents the highest pressure at that specific time point. The right panel shows the same data, but the colour scale remains constant throughout all time points. All presented values are for peak systole however blood flow dynamics were analysed for the entire cardiac cycle at each time point. All scale bars represent 100 µm.

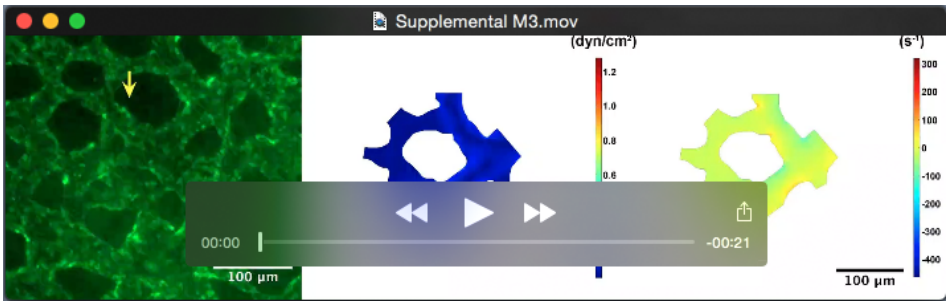

Movie 3. Shear stress and vorticity analysis around sprouting angiogenesis. Results of the shear stress and vorticity calculations at peak systole during sprouting are presented. The left panel shows the endothelial cell behaviour during the period of analysis. The centre panel shows the results for the shear stress calculations, with a constant colour scale for all time points. The right panel shows the results for the vorticity calculations, with a constant colour scale for all time points. All scale bars represent 100 µm.